Proceedings of the 21st ICSMGE, Vienna, Austria, 14 – 19 June 2026. Pistrol, Adam & Schweiger (eds.)
Published by: ÖGG, Austrian Society for Geomechanics, Salzburg, Austria, ISBN 978-3-9503898-4-5
https://doi.org/10.53243/ICSMGE2026-1468

Apparent protruding of tunnel shafts in Mexico City

Rodrigo Rodríguez, Marco Pérez, Carlos Sánchez, Darío Armendáriz, Rubén Domínguez, Gabriel Auvinet.
Institute of Engineering of UNAM, Mexico City, Mexico, rrodriguezr@iingen.unam.mx

ABSTRACT: The supply of potable water for Mexico City significantly depends on the pumping of underground aquifers through deep wells, causing regional subsidence in the lacustrine area. There is no short-term alternative foreseen to reduce this exploitation, thus the subsidence will persist, affecting deep foundations. Current numerical analyses do not always properly consider the long-term interaction between structures and soils undergoing regional subsidence. To address this, virtual elements that simulate this interaction (interfaces) are required. This study examines the behavior of access shafts to underground works constructed in the soft soil of the lake area of Mexico City, which suffer considerable apparent protruding with respect to the surrounding ground and affect nearby structures and roadways. Results of numerical modeling of this long-term behavior based on different considerations regarding the shear strength mobilized in the interface elements are presented.

KEYWORDS: Soft soil, regional subsidence, protruding, tunnel shafts, soil-structure interaction.

1 INTRODUCTION

1.1 *Regional subsidence*

The subsoil of Mexico City is subject to overexploitation of its aquifers, which leads to a reduction in interstitial pressures and, consequently, generates regional subsidence (RS). Nearly a century after its discovery by Roberto Gayol (1925) and more than seventy years after its explanation by Nabor Carrillo (1948), RS persists, causing differential settlements in various structures across Mexico City. This results in multiple impacts including damage to underground lining systems, apparent protruding of structures with deep or overcompensated foundations, and ground cracking in transition zones, all of which pose potential hazards.

Despite significant efforts, RS has not been successfully controlled, necessitating urgent solutions to preserve affected structures and reconsider strategies to mitigate future effects. Figure 1 shows the spatial variation of subsidence rates. Observations indicate that some areas of Mexico City have recorded subsidence rates approaching 40 cm/year.

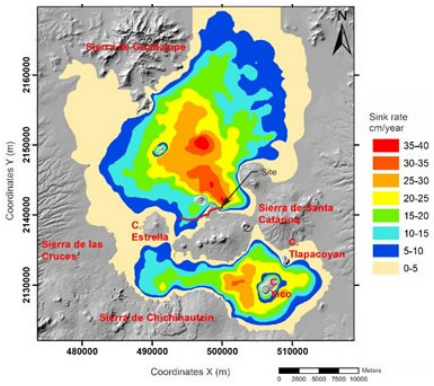

Figure 1. Mapping of rates of regional subsidence (Juárez *et al*., 2022)

1.2 *Mexico City's Drainage System*

In 1607, Viceroy Luis de Velasco approved Enrico Martínez's project to drain the Basin of Mexico, which included diverting the Cuautitlán River toward the Gulf of Mexico. Although constructed rapidly, the system proved inadequate and experienced collapses, leading to the construction of the trench known as "Tajo de Nochistongo" instead of a tunnel, a project that spanned 150 years (1637-1787). A new drainage project was approved in 1856, featuring the construction of the “Gran Canal del Desagüe del Valle de México” (Great Drainage Canal of the Valley of Mexico) and the Tequixquiac I Tunnel, inaugurated by President Porfirio Díaz in 1900.

By the early 1950s, differential settlements caused by RS had lowered the city's collectors below the level of Gran Canal, obstructing water flow and causing stagnation that led to significant flooding in central Mexico City during 1951 and 1952.

The construction of the deep drainage system began in 1967 with a capacity of 200 m³/s, marking a pivotal moment in the drainage and soil mechanics history of the Valley of Mexico (Auvinet *et al.,* 2016). The first phase was completed in 1975 with the Central Outfall (Emisor Central), featuring a 6.5 m diameter, 50 km length, and 23 shafts ranging from 50 to 237m in depth. Its route begins in Cuautepec and discharges into the Salto River, which joins the Tepeji River to form the Tula River that ultimately flows to the Endhó Dam and then to the Pánuco River and Gulf of Mexico.

Three main interceptors connect to the Central Outfall: The Centro-Poniente Interceptor (16 km long, 4 m diameter) running from Shaft 14 near the CFE Museum to Shaft 1; the Central Interceptor (7.78 km long, 5 m diameter) originating at Shaft 9 at the Monumento a la Raza and continuing along Avenida de los 100 Metros to Shaft 0; and the Oriente Interceptor (10.17 km long, 5 m diameter, 6 shafts) with a capacity of 100 m³/s from Gran Canal. After 1975, these interceptors were extended southward and interconnected via the Centro-Centro Interceptor.

Recent significant drainage projects include the Río de la Compañía Tunnel, Churubusco-Xochiaca Tunnel, Chimalhuacán II Tunnel, Canal General Tunnel, Emisor Poniente II Tunnel, and Emisor Oriente Tunnel.

In recent decades, several studies have analyzed tunnels, shafts, and their connections subjected to regional subsidence using numerical models; notable examples include the works of Arnau & Peña (2014), Auvinet et al. (2010), and Flores et al. (2016).

1.3 *Effects of Regional Subsidence on Shafts*

As previously mentioned, the decision to construct the deep drainage system in 1967 was driven by the need to mitigate potential differential settlements and maintain the designed slope.

Some shafts of the system were founded directly on the hard stratum, while others were positioned several meters above it. Currently, these shafts particularly those along the interceptors - exhibit apparent protruding and are beginning to affect adjacent roadways and neighboring properties. Several shafts located in parks and street intersections also show measurable protruding. This study examines two specific cases: first, Shaft 5 at the crossing of Francisco del Paso y Troncoso and Ignacio Zaragoza Avenues, showing 1.9 m of apparent

protruding measured from the shaft axis to a point 10 m away (Figure 2); second, Shaft 7 located in the park at intersection of Eduardo Molina and Antonio Ruiz Galindo Avenues, displaying 2.3 m of apparent emergence (Figure 3). Both shafts belong to the "Oriente Interceptor" of the deep drainage system.

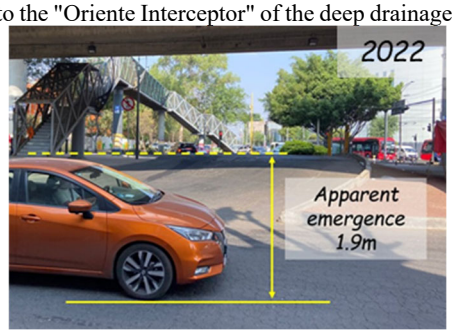

Figure 2. Shaft 5, Eastern Interceptor (Troncoso y Zaragoza).

Figure 3. Shaft 7, Eastern Interceptor (Eduardo Molina).

Figure 4 presents the geotechnical zoning chart showing the overall general sewerage system of Mexico City. The chart reveals that shafts of the Central, Oriente, and Centro-Centro Interceptors are located in Zone III, characterized by greater clay thickness and significant regional subsidence rates, as previously illustrated in Figure 1.

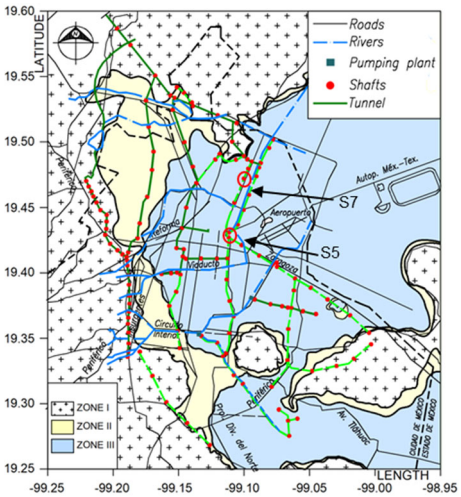

Figure 4. General sewerage system of the Mexico City (Modified from Hydraulic Engineering in Mexico, 1991).

2 GEOTECHNICAL INFORMATION ON SHAFTS

The publication "Failures of Shafts and Tunnels in Soft Soils" (Moreno and Schmitter, 1981) describes the two case studies and presents the soil resistance profiles. The shafts have a diameter of 9 m with wall thickness of 0.6 m. Both structures were built using the SOLUM technique, as mentioned in Moreno A. (19991). Shaft 5 is founded 3 m above the first hard layer. In contrast, Shaft 5 is founded directly on the first hard layer (Figure 5).

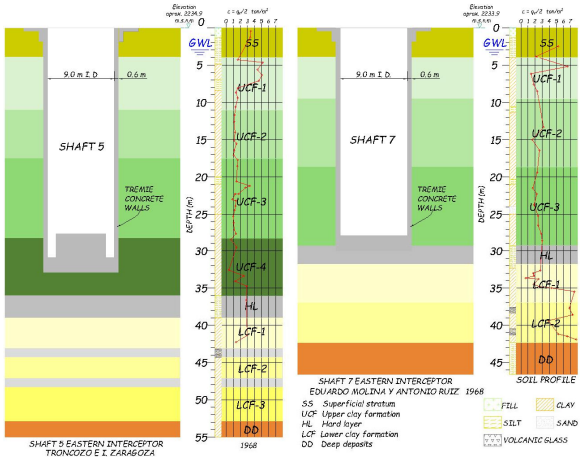

Figure 5. Geotechnical profiles of the S5 and S7 Shafts of the Eastern Interceptor.

This information was complemented with nearby boring data. Figure 6 presents borings near Shaft 5 from 1951, 1968, 1997, and 2017. Figure 7 shows three borings near Shaft 7, corresponding to years 1948, 1968 (start of construction), and 2018. In both cases, the data reveal changes in ground elevation and variations in thickness of the upper and lower clay formations (UCF and LCF, respectively).

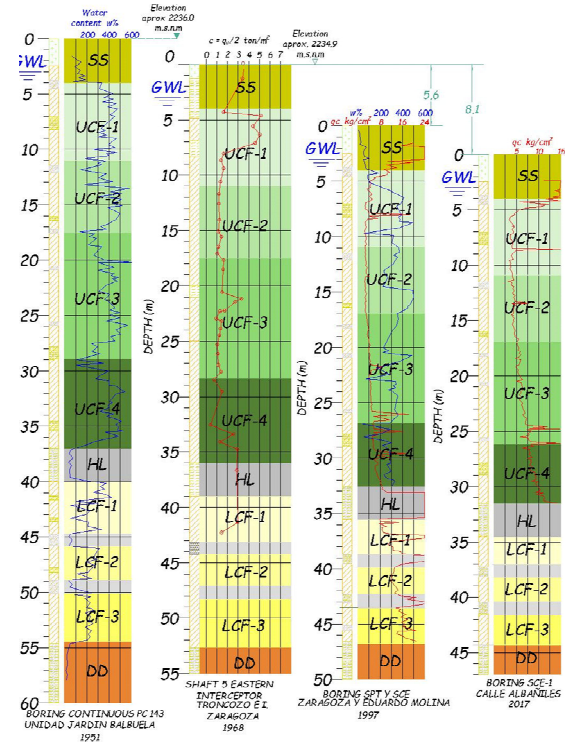

Figure 6. Borings near shaft 5.

Based on this information, the geotechnical models for Shafts S5 and S7 presented in Table 1 and 2 were developed using the Soft Soil model for the compressible lacustrine clays and the Mohr–Coulomb model for the stiffer layers and the soil–concrete interface. The Soft Soil model is appropriate for reproducing consolidation-driven settlements due to its formulation based on the Modified Cam-Clay framework, though it is less suitable for excavation stages where stress paths become highly non-linear. In contrast, the Mohr–Coulomb model provides a simpler and robust representation for stiff soils and for simulating adhesion at the shaft walls. Table 3 presents the initial pore pressure distributions used for Shafts S5 and S7.

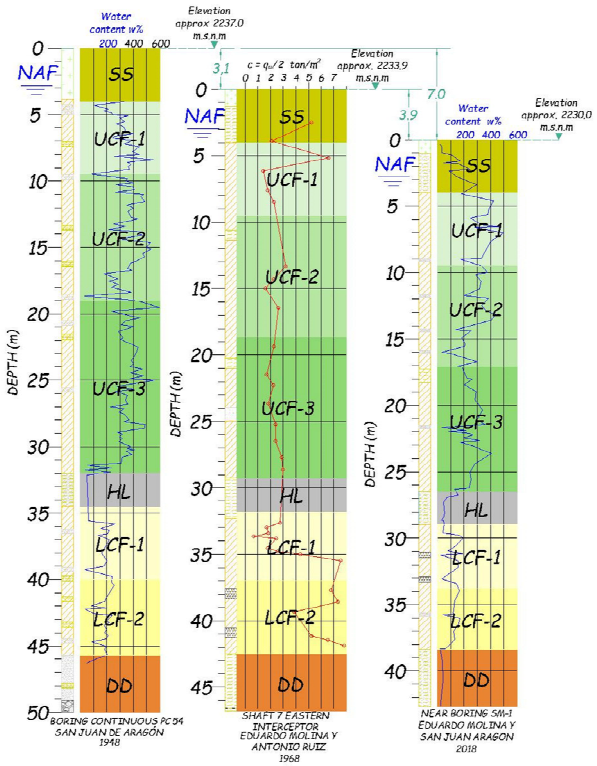

Figure 7. Borings near shaft 7.

Table 1. Geotechnical model for Shaft S-5.

GU	γ (kN/m³)	e_0	c_c	c_r	E (MPa)	c (kPa)	ϕ (°)
SS	13.7	0.5	-	-	4.5	55	30
UCF-1	11.5	7.7	6.1	0.61	-	0	35
UCF-2	11.3	8.0	6.2	0.62	-	0	35
UCF-3	11.4	8.1	6.0	0.60	-	0	35
UCF-4	11.3	8.5	6.7	0.67	-	0	35
HL	16.0	0.5	-	-	25	100	45
LCF-1	12.0	4.0	4.1	0.41	-	0	35
LCF-2	12.0	3.8	3.9	0.39	-	0	35
LCF-3	12.3	3.0	3.5	0.35	-	0	35
DD	18.0	0.5	-	-	30	150	45

Table 2. Geotechnical model for Shaft S-7.

GU	γ (kN/m³)	e_0	c_c	c_r	E (MPa)	c (kPa)	ϕ (°)
SS	15.0	0.5	-	-	4.5	55	30
UCF-1	11.5	7.8	5.9	0.8	-	0	35
UCF-2	11.4	6.1	6.1	0.6	-	0	35
UCF-3	11.4	6.9	5.7	0.4	-	0	35
CD	16.0	0.5	-	-	25	100	45
LCF-1	13.0	4.2	2.3	0.2	-	0	35
LCF-2	13.7	3.8	1.9	0.2	-	0	35
DD	18.0	0.5	-	-	30	150	45

Table 3. Pore pressure initial for shafts S5 and S7.

Depth (m) Shaft 5	Pore Pressure (kPa) Shaft 5	Depth (m) Shaft 7	Pore Pressure (kPa) Shaft 7
3.0	0.0	2.8	0.0
4.0	10.0	4.0	12.0
11.0	80.0	9.5	57.7
17.5	145.0	18.7	130.3
28.4	225.4	25.1	178.3
36.0	313.5	29.3	209.8
39.0	343.5	31.8	209.8
43.1	386.0	37	265.0
44.2	397.0	40	295.0
47.1	425.0	42.3	321.2
48.1	435.6		
52.1	477.0		

3 NUMERICAL EVALUATION OF APPARENT PROTRUDING OF SHAFTS

3.1 *Numerical modeling*

The numerical modeling was conducted based on geotechnical models, piezometric conditions, and shaft geometry. The finite element code from the commercial software PLAXIS 2D, axisymmetric version (2024), was used for the analysis.

Figures 8 and 9 show the finite element meshes for shafts S5 and S7. The horizontal dimension of the finite element meshes were extended to prevent unrealistic boundary effects on the results. In each case, geotechnical information was available up to the depths of the deep deposits (DD). A linear elastic model was used to represent the mechanical behavior of the shaft structural elements. In these initial models, the elasto-plastic behavior of concrete was neglected. The elastic modulus was calculated from the unconfined compressive strength ($f'c$ = 210 kg/cm²) and the unit weight was considered as 24 kN/m³.

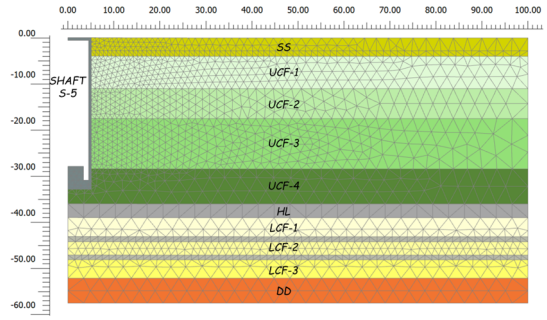

Figure 8. Finite element mesh for shaft 5.

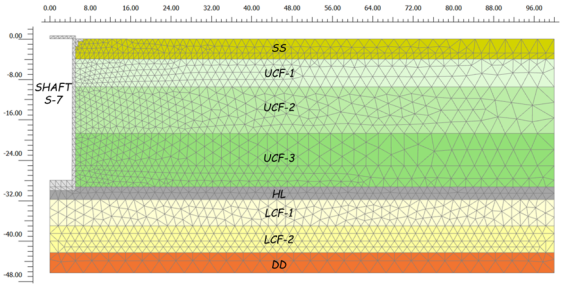

Figure 9. Finite element mesh for shaft 7.

Three analysis stages were generated: the first to establish initial stress conditions in the ground (E0), the second to simulate complete shaft construction (E1), and the third to analyze the effects of regional subsidence (E2).

Interface elements were incorporated between the shafts and adjacent soil (Figure 10). These elements allow representation of the soil-concrete adherence and potential relative displacements between these materials.

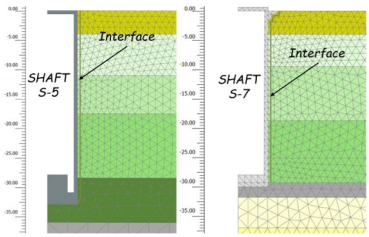

Figure 10. This is Interface element between the shaft and the adjacent soil in shafts S-5 and S-7.

Initially, the adherence was represented using the R_{inter} factor, which reduces soil properties (Equations 1 and 2) only at the geometric location of the interface. Parametric analyses were therefore conducted to represent the current protruding condition of the shafts and determine the appropriate value for this parameter.

$$C_i = R_i c_s \quad (1)$$

$$\varphi_i = \tan^{-1}(R_i \tan \varphi_s) \quad (2)$$

where: c_s and φ_s are the cohesion and internal friction angle of the soil; C_i and φ_i are the cohesion and friction angle at the interface; and R_i is the reduction factor.

Additionally, a Mohr-Coulomb material type was assigned to the interface to represent the adherence between the soil and shaft wall. Equation 3 was used to calculate the adherence, while Equation 4 was used to calculate the undrained shear strength of soft soils.

$$\eta = 0.4\sqrt{\sigma_z'/c_u} \quad (3)$$

$$c_u = \frac{\sigma_x' + \sigma_z'}{2} sen\varphi \quad (4)$$

where: c_u is the undrained shear strength of the soil; σ_x' and σ_z' are the effective horizontal and vertical stresses; and φ is the internal friction angle.

3.2 *Regional Subsidence in Free-Field Conditions*

To numerically simulate regional subsidence (RS) under free-field conditions, target pore pressure distributions (Table 4) were determined to generate the observed settlements and heaves shown in Figures 6 and 7, corresponding to the dates when nearby borings were performed. Therefore, the drawdown is not expressed as a uniform percentage relative to an initial pore pressure, but rather as a final pore pressure profile adjusted layer by layer to match the accumulated regional consolidation.

Figures 11 and 12 demonstrate that the drawdowns associated with the target pore pressures (proposed in Table 4) produce vertical surface displacements in the models that closely match those observed when comparing the profiles in Figures 6 and 7, respectively. For Shaft 5, the drawdowns for the periods between 1968-1997 and 1997-2017 showed differences of 5.4 m and 8.1 m, respectively. In the case of Shaft 7, the drawdown corresponding to the period from 1968 to 2018 resulted in a 3.8 m difference

Table 4. Target pore pressure for shafts S5 and S7.

Depth (m) Shaft 5	Pore Pressure (kPa) Shaft 5	Depth (m) Shaft 7	Pore Pressure (kPa) Shaft 7
3.0	0.0	2.8	0.0
4.0	10.0	4.0	10.0
11.0	73.0	9.5	56.0
17.5	125.0	18.7	70.0
28.4	130.5	25.1	81.0
36.0	111.5	29.3	89.0
39.0	173.6	31.8	89.0
43.1	154.9	37	140.5
44.2	199.0	40	168.4
47.1	230.9	42.3	146.5
48.1	235.9		
52.1	217.5		

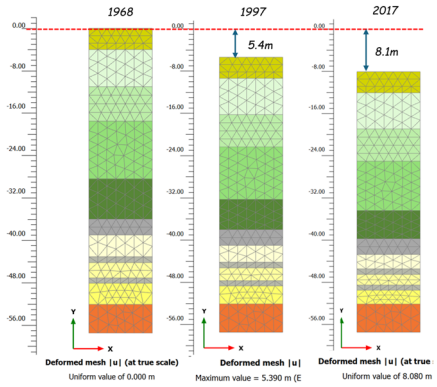

Figure 11. Regional subsidence model for the case of shaft 5.

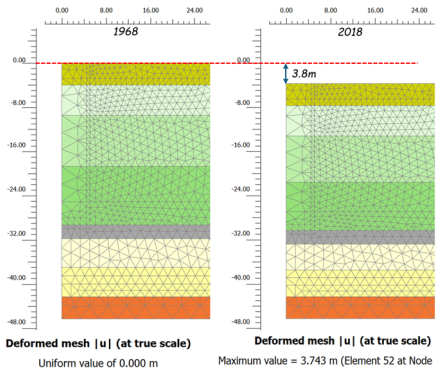

Figure 12. Regional subsidence model for the case of shaft 7.

3.3 *Effect of Regional Subsidence on Shafts*

Figure 13 shows the deformed meshes corresponding to calculation stage E2 for shafts S-5 and S-7 using a R_{inter} value of 1. In both cases, the regional subsidence (RS) occurring away from the shafts matches the behavior observed in Figures 11 and 12. The apparent protruding measured in shafts S-5 and S-7 were 2.1 m and 2.3 m respectively (EM = Emergence Measured), values that correspond with field measurements.

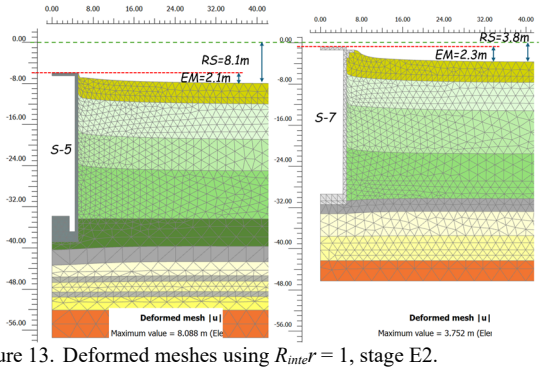

Figure 13. Deformed meshes using R_{inter} = 1, stage E2.

Figure 14 presents the plastic points that appear in approximately the first 24 meters of the soil-shaft interface. This plastic condition indicates that the shear stresses generated by the negative friction associated with RS exceed the soil's strength at the interface zone. However, due to the continuity condition implicit in using R_{inter} = 1, no soil sliding occurs along the shaft walls.

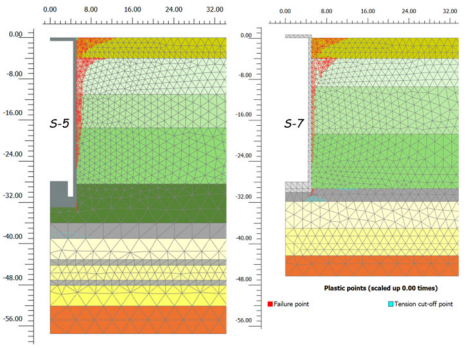

Figure 14. Plastic points at the shaft-soil contact due to negative friction, Rinter = 1.

Figures 15 and 16 show the ground surface deformations for shafts S-5 and S-7 when interface R_{inter} factors ranging from 1 to 0.1 were applied. The results demonstrate that R_{inter} values of 0.6-0.7 for Shaft S-5 and 0.5-0.6 for Shaft S-7 approximately reproduce the emergence values shown in Figures 3 and 4. The slight difference in optimal R_{inter} ranges between cases relates to their foundation conditions: Shaft S-7 is founded directly on the hard layer while Shaft S-5 rests on the upper clay formation (UCF) 3 meters above the hard layer. Consequently, the effect of RS on shaft walls is more pronounced for Shaft S-7, requiring less strength reduction to match the observed uplift values.

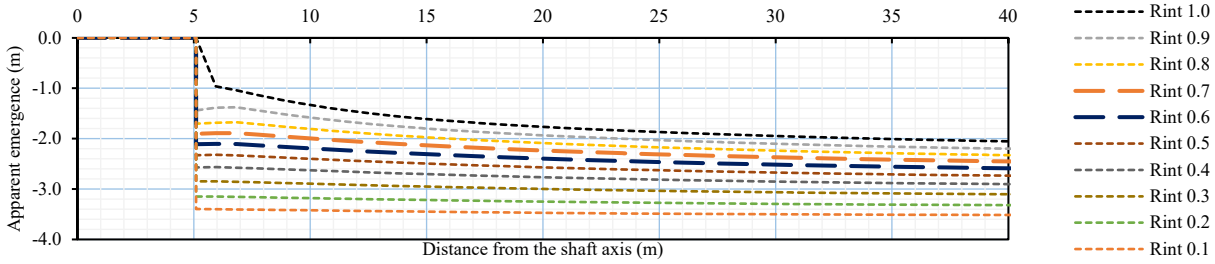

Figure 15. Apparent emergence from the shaft S-5.

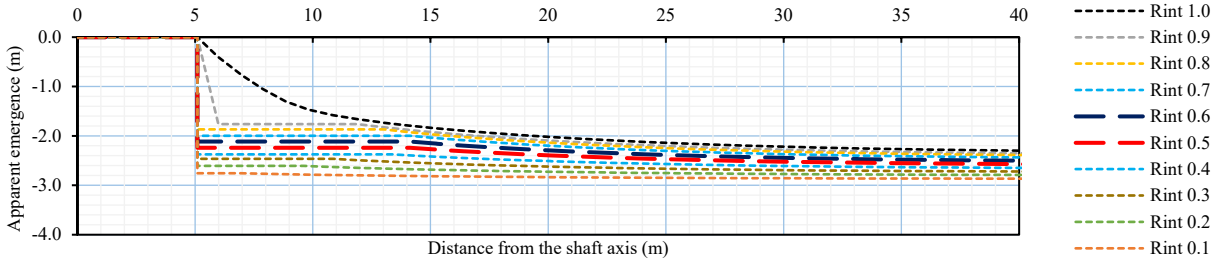

Figure 16. Apparent emergence from the shaft S-5.

Figure 17 shows the deformed meshes corresponding to calculation stage E2 for the cases of shafts S-5 and S-7. In both cases, the adherence values shown in Tables 5 and 6, respectively, were used. It is observed that the RS, away from the shafts, is similar to those observed in Figures 12 and 13, and that the apparent protruding obtained in both shafts are 2 m. These emergencies are of a similar order of magnitude to those observed in the field. Figures 18 and 19 show the deformed meshes on the ground surface of shafts S-5 and S-7, when adherence and R_{inter} values of 0.6-0.7 and 0.5-0.6, respectively, were applied to their interfaces. It is observed that the protruding generated with R_{inter} = 0.6 is like those generated using the calculated adherences.

Figure 20 shows the plastic points generated by negative skin friction corresponding to the RS. They are observed in the first 32 m (approximately), at the contact point between the soil and the shaft. This plasticity condition indicates that the limit adherence imposed in the soil-shaft interface is exceeded.

Table 5. Adherences shaft 5.

UG	Depth (m)		Thickness	c_u	Ad
	De	A	(m)	(kPa)	(kPa)
SS	0.0	4.0	4.0	60	19.9
UCF-1	4.0	11.0	7.0	21	16.0
UCF-2	11.0	17.5	6.5	25	19.0
UCF-3	17.5	28.4	10.9	36.	27.4
UCF-4	28.4	36.0	7.6	43	34.1
HL	36.0	39.0	3.0	-	-

Table 6. Adherences shaft 7.

UG	Depth (m)		Thickness	c_u	Ad
	De	A	(m)	(kPa)	(kPa)
SS	0.0	4.0	4.0	60	21.0
UCF-1	4.0	9.5	5.5	24.5	18.2
UCF-2	9.5	18.7	9.2	34.5	26.1
UCF-3	18.7	29.3	10.6	50	37.9
HL	29.3	31.8	2.5	-	-

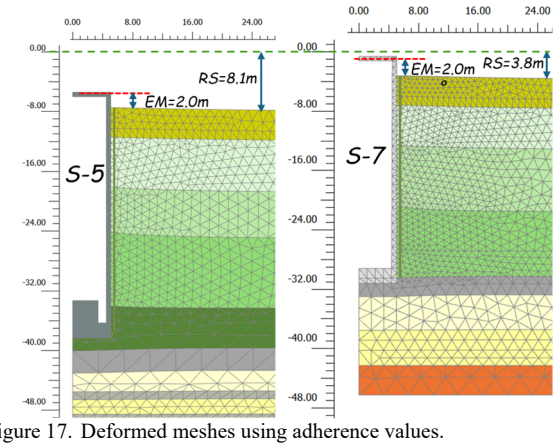

Figure 17. Deformed meshes using adherence values.

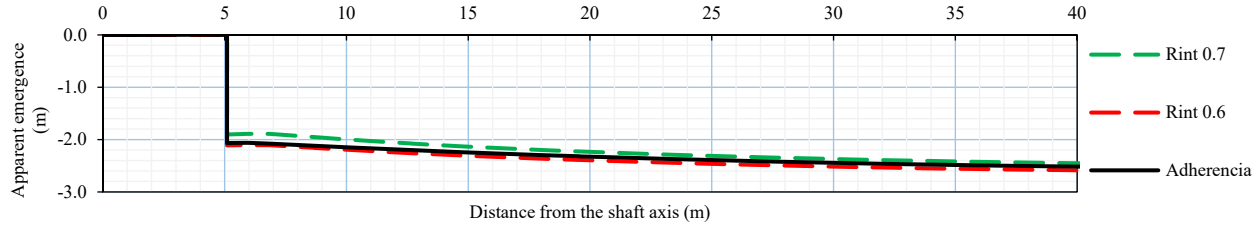

Figure 18. Apparent protruding of shaft S-5.

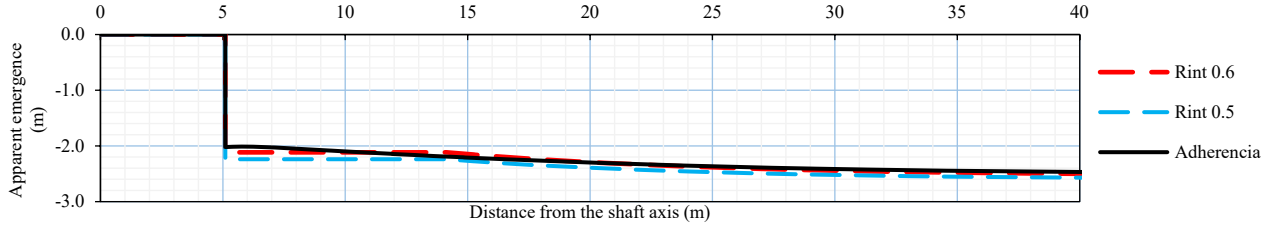

Figure 19. Apparent protruding of shaft S-7.

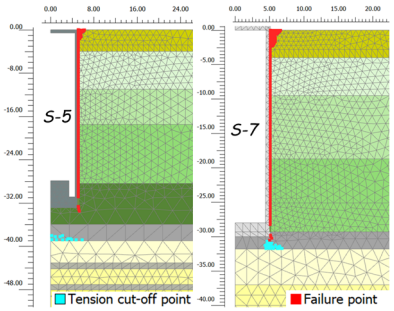

Figure 20. Plastic points at the shaft-ground contact.

Therefore, the interfaces placed at the soil-shaft contacts, modeled with calculated adherences and R_{inter} parameter values close to 0.6, allow for the generation of soil relative displacement that accurately represents the apparent protruding observed in the field.

The II-UNAM continues to perform numerical modeling to represent the behavior of other shafts, with the aim of verifying whether R_{inter} values close to 0.6 allow the emergence conditions at each site to be reproduced. Numerical simulations are also being carried out using other interface representations, such as normal and tangential stiffnesses, as well as other constitutive models to represent soil behavior.

This criterion of incorporating an interface at the soil–shaft contact to evaluate apparent protrusion can be applied both in future designs and in maintenance work for shafts that have already emerged, particularly those that affect roadways. Several of these structures have been reconfigured to mitigate the protrusion; however, they will likely continue to exhibit this phenomenon over time.

4 CONCLUSIONS

The exploitation of aquifers in Mexico City has led to regional subsidence, a problem that has persisted for almost a century and continues to affect urban infrastructure.

The construction of the deep drainage system, initiated in 1967, was a measure to mitigate the effects of subsidence. However, some shafts have presented apparent protruding, which has begun to affect roads and surrounding areas.

Detailed studies have been conducted using geotechnical models and PLAXIS 2D software to analyze the behavior of the shafts under current subsidence conditions. These models have made it possible to accurately represent the protruding observed in the field.

Shafts 5 and 7, despite being similar in design, show different behaviors due to their location relative to the subsoil first hard layer. Shaft 7, which is located above the hard layer, is more affected by regional subsidence compared to shaft 5, which is located 3 meters above the hard layer.

Studies suggest that adherence and resistance at the interface between the soil and the shafts (R_{inter}) values are crucial for accurately representing apparent emergence. R_{inter} values close to 0.6 have been effective in modeling observed field conditions.

5 REFERENCES

Arnau, O., y Peña, F. (2014). “Evaluación de daños estructurales en conexiones túnel– lumbrera ocasionados por asientos diferenciales “ XIX Congreso Nacional de Ingeniería Estructural, SMIE, Puerto Vallarta, Jalisco.

Auvinet, G., Rodríguez, J.F. and Rangel, J.L. (2010). Construction of deep tunnel shaft in Mexico City sotf clays by the flotation method, Acta Geotechnica. (2010) 5: 63 doi:10.1007/s11440-010-0115-2

Auvinet, G., Méndez, E. y Juárez, M. (2016). El subsuelo de la Ciudad de México/The subsoil of Mexico City, Vol. III. ISBN 978-607-02-8198: UNAM.

Carrillo, N. (1948). “Influence of Artesian Wells on the Sinking of México City”, Proceedings, Second International Conference on Soil Mechanics and Foundation Engineering, Vol. 2, pp 156-159, Rotterdam, Netherlands.

Dirección General de Obras Hidráulicas. (1969). “Interceptores profundos y el emisor central”, Departamento del Distrito Federal, México D. F.

Flores, F. A., Gordillo, N. O., Enríquez, O., De la Rosa, J. M., Guasch, J. C. (2016) “Evaluación del efecto por hundimiento regional en conexiones túneles-lumbreras” XXVIII Reunión nacional de Ingeniería Geotécnica. Yucatán, México.

Gayol, R. (1925). “Estudio de las perturbaciones que en el fondo del Valle de México ha producido el drenaje de las aguas del subsuelo …”, Primera parte, Revista Mexicana de Ingeniería y Arquitectura, Vol. III, No. 3, pp. 96-132, México, agosto 1925.

Juárez, M., Auvinet, G., Román, H., y Méndez, E. (2022) “Predicción del hundimiento regional en el valle de México” XXXI Reunión nacional de Ingeniería Geotécnica. Guadalajara, México.

Moreno A. and Schmitter J. (1981). “Failures of shafts and tunnels in Soft Soils”, Soft-Ground Tunneling. Failures and Displacements. Balkeman, Rotterdam, P: 23-32

Moreno A. (1991). “Lumbreras y túneles en suelos”, Trabajo de ingreso a la academia de ingeniería. México, P: 6-13

Sistemas de aguas de la Ciudad de México (2012) “El gran reto del agua en la Ciudad de México” SACMEX, Ciudad de México., P: 53-86